PHYSICAL REVIEW B **94**, 024102 (2016)

Avalanche criticalities and elastic and calorimetric anomalies of the transition from cubic Cu-Al-Ni to a mixture of 18*R* and 2*H* structures

Eduard Vives,[1] Jordi Baró,[1] María Carmen Gallardo,[2] José-María Martín-Olalla,[2] Francisco Javier Romero,[2] Sarah L. Driver,[3] Michael A. Carpenter,[3] Ekhard K. H. Salje,[3] Marcelo Stipcich,[4,5] Ricardo Romero,[4] and Antoni Planes[1]

[1]*Departament d'Estructura i Constituents de la Matèria, Facultat de Física. Universitat de Barcelona, Diagonal, 647, E-08028 Barcelona, Catalonia, Spain*

[2]*Departamento de Física de la Materia Condensada, Universidad de Sevilla, P.O. Box 1065, E-41080 Sevilla, Spain*

[3]*Department of Earth Sciences, University of Cambridge, Downing Street, Cambridge CB2 3EQ, United Kingdom*

[4]*IFIMAT, Universidad del Centro de la Provincia de Buenos Aires and CICPBA, Pinto, 399, 7000 Tandil, Argentina*

[5]*Consejo Nacional de Investigaciones Científicas y Técnicas, A. Rivadavia 1917, Buenos Aires, Argentina*

(Received 24 February 2016; revised manuscript received 10 May 2016; published 5 July 2016)

We studied the two-step martensitic transition of a Cu-Al-Ni shape-memory alloy by calorimetry, acoustic emission (AE), and resonant ultrasound spectroscopy (RUS) measurements. The transition occurs under cooling from the cubic (β, $Fm3m$) parent phase near 242 K to a mixture of orthorhombic $2H$ and monoclinic $18R$ phases. Heating leads first to the back transformation of small $18R$ domains to β and/or $2H$ near 255 K, and then to the transformation $2H$ to β near 280 K. The total transformation enthalpy is $\Delta H_T = 328 \pm 10$ J/mol and is observed as one large latent heat peak under cooling. The back-transformation entropy under heating breaks down into a large component $18R$ to β at 255 K and a smaller, smeared component of the transformation $2H$ to β near 280 K. The proportions inside the phase mixture depend on the thermal history of the sample. The elastic response of the sample is dominated by large elastic softening during cooling. The weakening of the elastic shear modulus shows a peak at 242 K, which is typical for the formation of complex microstructures. Cooling the sample further leads to additional changes of the microstructure and domain wall freezing, which is seen by gradual elastic hardening and increasing damping of the RUS signal. Heating from 220 K to room temperature leads to elastic anomalies due to the initial transformation, which is now shifted to high temperatures. The transition is smeared over a wider temperature interval and shows strong elastic damping. The shear modulus of the cubic phase is recovered at 280 K. The phase transformation leads to avalanches, which were recorded by AE and by time-resolved calorimetry. The cooling transition shows very extended avalanche signals in calorimetry with power-law distributions. Cooling and heating runs show AE signals over a large temperature interval above 260 K. Splitting the transformation into two martensite phases leads to power-law exponents $\varepsilon \sim 2$ ($\beta \leftrightarrow 18R$) and $\varepsilon \sim 1.5$ ($\beta \leftrightarrow 2H$) while the phase mixture shows an effective AE exponent of 1.7.

DOI: 10.1103/PhysRevB.94.024102

I. INTRODUCTION

Martensitic transitions are diffusionless structural transitions that involve a change from high to low symmetry phases dominated by a shear mechanism [1]. Usually, these transitions show athermal character to some approximation, and thus proceed via a sequence of avalanches associated with discontinuities of the order parameter that reflect the fact that, when externally driven, the system jumps across a sequence of metastable states. Avalanches are a consequence of dynamical constraints imposed by nonhomogeneities associated with both intrinsic disorder such as lattice defects, impurities, or by jamming, together with long-range interaction arising from elastic compatibility constraints [2–4]. Avalanches in many such systems occur with the absence of characteristic time and size scales. This behavior defines the so-called avalanche criticality where the dynamics of the transformation process is characterized by a power law of the avalanche size or energy probability distribution function. Under athermal conditions, the power-law exponents have been argued to depend on the driving mechanism [5,6] and computer simulations found no shifts of the exponents [7] when the microstructural transformation process remained topologically invariant. This result suggests that exponents may change as function of variant multiplicity, which is the number of equivalent structural domains that can occur at the transition [8]. This reflects the idea that by increasing variant multiplicity, the system is able to find more paths connecting high- and low-temperature phases, which may affect exponents of the avalanche size and energy. Recently the effect of internal twinning of martensitic variants on propagation dynamics has also been suggested to influence avalanche dynamics during stress-induced transformation to an orthorhombic martensite in Cu-Al-Ni [9]. To further clarify the influence of symmetry effects on avalanche criticality, we study avalanches in the thermally induced martensitic transition of a Cu-Al-Ni alloy, which transforms to a mixture of monoclinic and orthorhombic phases involving variant multiplicities of 12 and 6. We show that the power-law exponents do indeed change for different heating and cooling protocols due to history-dependent effects on the selected transition paths.

We monitor martensitic avalanches from acoustic emission (AE) and calorimetric measurements. AE originates from fast local changes of strain fields across propagating interfaces. It is a very sensitive technique that allows the detection of weak events over a wide range of length scales from nanometers to microns. Acoustic AE waves carry temporal and spatial information related to the source of the acoustic emission, and have been used extensively in the past to study

martensitic phase transitions (see, for instance, Ref. [10,11]). Recently, by modeling AE waveforms of the acoustic events it has been shown that the transformation from cubic to orthorhombic in Cu-Al-Ni occurs on a faster timescale than the transformation to the monoclinic phase [12]. Here we focus on another aspect of the transition mechanism, namely the collective dynamics of the transition from the view of statistical mechanics. We measure the energy and amplitude of AE events during the transformation processes [8] and combined these measurements with calorimetric and RUS measurements, which allows us to distinguish between two different transformation mechanisms.

Cu-Al-Ni belongs to the family of Cu-based Hume-Rothery shape-memory alloys. In this class of alloys, fast cooling from the high-temperature (disordered bcc phase) stability region prevents the formation of equilibrium phases and thus enables retaining of an ordered (nearest- and next-nearest-neighbor ordering) cubic phase (usually denoted β phase) at (or close to) room temperature. After further cooling, this long-living metastable phase undergoes a martensitic transition. This material has been the subject of active research during recent years, since associated with the martensitic transition, it displays interesting shape memory and superelastic properties [13]. Problems such as the influence of aging [14,15] and cycling [16] on the transition and martensitic microstructure, and the elastic behavior above and below the transformation [17,18] among others, have been studied in detail due to their relevance in relation to potential technological applications of this material.

In Cu-based alloys, phase stability is largely controlled by the electron concentration, e/a [19]. In particular, the actual martensitic structure is sensitive to fine tuning of the electron concentration e/a [20]. In Cu-Al-Ni the stability boundary separating the monoclinic $18R$ from the orthorhombic $2H$ phase has been predicted at $e/a \sim 1.53$ [21]. It has been reported that both monoclinic and orthorhombic phases can coexist [22–24] close to this critical electron concentration. The existence of this coexistence region is also favored by the fact that the stresses associated with the occurrence of orthorhombic variants at the onset of the temperature-driven transition may induce the transformation towards the monoclinic phase [25]. Thermally induced transitions equally occur so that the methodology of the investigation of ferroelastic phase transitions becomes applicable [26] while the athermal nature of the phases remains approximately preserved over limited temperature intervals [27].

II. EXPERIMENT

A Cu-Al-Ni polycrystalline sample was prepared by alloying 99.99% purity copper, aluminum, and nickel. Small pieces with appropriate masses (weighted with a precision of 0.1 mg) of each metal were cut and were melted by means of a W-2%Th electrode vacuum arc furnace into a water-cooled copper crucible under a partial argon atmosphere. The sample was remelted at least eight times in order to reach a high homogeneity degree. After solidification, the Cu-Al-Ni alloy was homogenized at 1073 K for about two days. It was then quenched in water and annealed at room temperature for some weeks. This heat treatment ensures a highly ordered

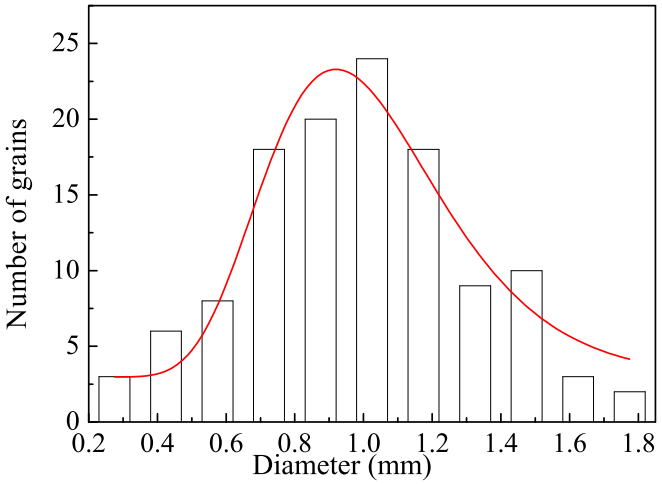

FIG. 1. Grain size distribution of the studied sample. The continuous line is a log-normal fit.

state, free from internal stresses and with minimum vacancy concentration. This heat treatment resulted in a large grain size with average diameter of about 1 mm (see Fig. 1). The composition was obtained from EDX measurements to be $Cu_{68.1}Al_{28.1}Ni_{3.8}$ ($e/a = 1.56$). At high temperature, the sample displays an $L2_1$ ($Fm3m$) cubic structure (β phase). For calorimetric and AE measurements the same specimen was used. It was cut from the ingot with a low-speed diamond saw. The specimen is 2.4 mm tall and has a flat nearly rectangular base of 53.5 mm^2. The corresponding mass is 0.9921 g. For RUS measurements we cut a slice of 4 mm × 2.4 mm × 1 mm, parallel from one side of the specimen used for calorimetry and AE experiments.

The heterogeneous strains generated by the polycrystalline nature of the sample were analyzed by x-ray diffraction using a William-Hall analysis. The resulting William-Hall plots confirm large grain sizes and moderate strain broadening. The heterogeneous strain along the cubic main axes {100} is 2.4% and 0.5% along {110} directions. This means that grains are squeezed along the {100} directions but rather unstressed along the {110} directions. This is related to the direction of the shear mechanism leading to the martensitic structure from the parent cubic phase [20]. The overall strain effect is, thus, rather small and not unusual for martensitic transformations.

Measurements of heat flux ϕ were performed using a high-resolution conduction calorimeter, which has been described elsewhere [28]. The sample is pressed between two identical heat flux meters, which are made from 50 chromel-constantan thermocouples connected in series, with the wires placed in parallel lines. The flux meters are thermally coupled to a large calorimetric block. The block is placed into a hermetic outer case under vacuum (10^{-7} torr). The temperature of the calorimetric block is recorded by means of a platinum resistance thermometer.

Heat fluxes were measured with a resolution <0.1 μW. Due to the high thermal inertia of the calorimeter block, it was possible to perform experiments at very low-temperature rates, r, in the range 10^{-4}–10^{-5} K/s. Temperature fluctuations of the calorimeter block were smaller than 10^{-6} K. The system works as differential thermal analysis (DTA) device during cooling

and heating runs. The electromotive force provided by the flux meters, which is proportional to the heat flux, was recorded by a nanovoltmeter Keithley K2182 at a sampling rate of 12.5 Hz. The integral of the flux above a suitable baseline is proportional to the excess enthalpy of the sample [29].

The experimental arrangement for AE measurements is based on a PCI-2 acquisition system (Europhysical Acoustics), working at a nominal time resolution of 40 MHz. The sample was mounted on the top of a copper block situated inside a double Faraday cage constituted of copper and iron shielding layers. A piezoelectric sensor (R15LT transducer, encapsulated in stainless steel) was acoustically coupled to the upper surface of the sample by a thin layer of petroleum jelly. The signal from the transducer was amplified (60 dB), band filtered between 200 kHz and 1 MHz, and transferred to the acquisition system. For identification of AE events, a threshold above the (unavoidable) instrumental noise was fixed at 24 dB. An event i was assumed to start with the first crossing of the threshold at time t_i. The end of the event, $t_i + \Delta t_i$, is determined when the voltage crosses the threshold in the downward direction and remains below threshold for more than a preset detection time of 100 μs in our experiments. The energy of the events is determined by numerical integration of the square voltage during the duration Δt_i, normalized by a reference electric resistance of 10 kΩ. The AE activity is defined as the number of events per unit time measured over large enough intervals (of the order of the second) so that this quantity can be compared with more macroscopic measurements such as calorimetry. A corresponding AE energy can also be defined as the sum of the energies of the events emitted over these large intervals.

The principles of RUS have been described in detail by Migliori and Sarrao [30] and Migliori and Maynard [31]. RUS is used to measure the resonant frequencies of normal modes of vibration of a material in the frequency region $\sim$ 0.1–2 MHz. In the low-temperature RUS arrangement used for the experiments described here, the sample sat lightly between piezoelectric transducers in a sample holder, which was lowered into an orange helium flow cryostat with a few mbars of helium as exchange gas [32]. Acoustic resonances of the sample were excited by sending an ac electric signal to one of the transducers, and were detected by the second transducer. Individual spectra, consisting of 130 000 data points, were collected in cooling and heating sequences, including a thermal equilibration period of 20 min at each temperature. Spectra were analyzed off line using the software package IGOR (Wavemetrics) to fit selected peaks with an asymmetric Lorentzian function. The square of the resonance frequency, f, scales with the elastic constants which determine a given mode and these, in turn, depend primarily on shearing motions. The peak width at half height, Δf, provides a measure of acoustic loss through the inverse mechanical quality factor, $Q^{-1} = \Delta f/f$.

III. RESULTS

DTA traces, defined as the ratio, ϕ/r, of heat flux and temperature rate, were obtained for heating and cooling runs. Two values of the temperature rate were used, $r = 0.04$ K/h ($\sim 10^{-5}$ K/s) and $r = 0.25$ K/h ($\sim 7 \times 10^{-5}$ K/s). Typical results are shown in Fig. 2. The direct transformation (cooling run) is characterized by a broad anomaly of the heat flux between 250 K and 230 K with a large number of spikes over a smaller temperature interval at the upper end of the broad anomaly. The reverse transformation (heating data) shows a smeared anomaly between 235 K and 260 K where a small number of weak spikes are superimposed, followed by a large number of strong heat flux peaks in the temperature interval between 265 K and 295 K. This suggests that on heating the transition is split into two different stages.

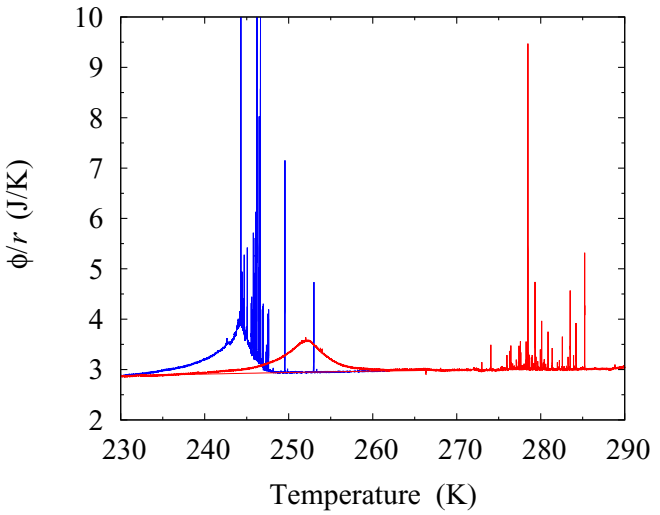

FIG. 2. DTA traces for heating (red) and cooling (blue) experiments. Data corresponding to cooling experiments have been changed in sign to allow a better comparison to heating data.

Integration of the DTA trace gives the transition enthalpy (Fig. 3), $\Delta H_T = 328 \pm 10$ J/mol. The low-temperature transformation (smooth anomaly with some spikes) accounts for 94% of total enthalpy. The high-temperature transformation accounts for the remaining 6%. The fraction of enthalpy as function of the temperature $\Delta H(T)/\Delta H_T$ is taken as measure for the transformed fraction $x(T)$.

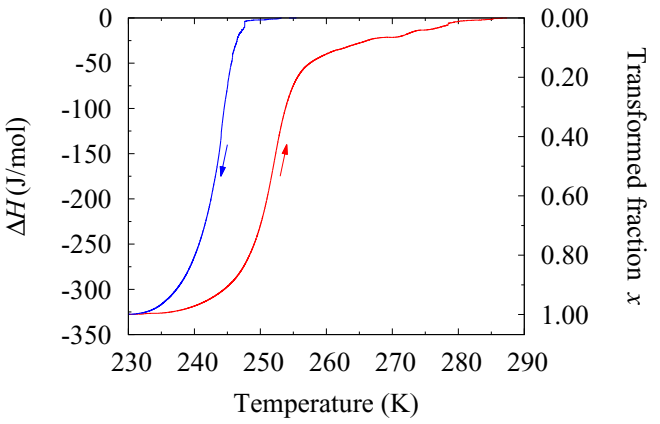

FIG. 3. Integrated transition enthalpy for heating (red) and cooling (blue) runs. The total enthalpy change is identical within experimental errors. The right scale gives the corresponding transformed fraction.

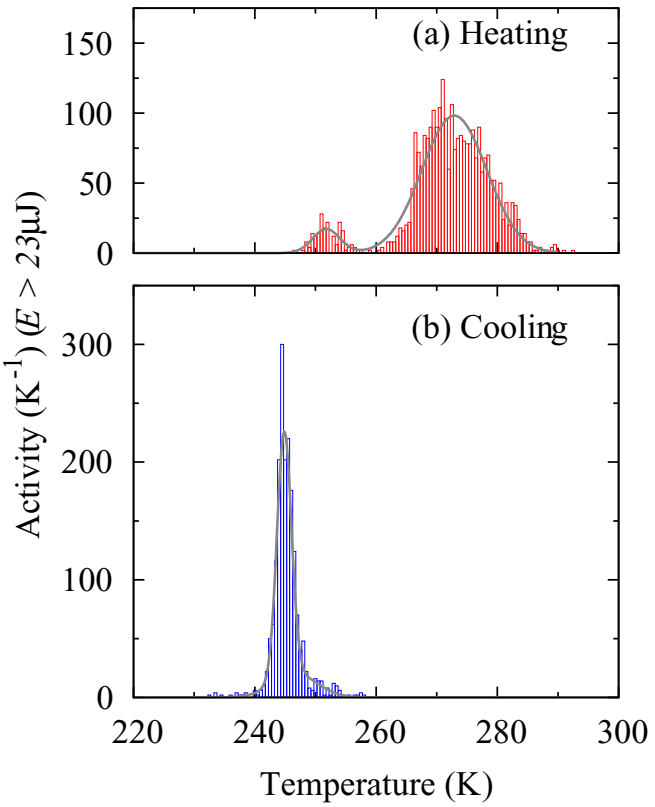

FIG. 4. Activity plots of avalanches obtained from calorimetric measurements during (a) heating and (b) cooling runs. Activity is measured by counting the number of spikes larger than 23 μJ in intervals of half a Kelvin. Smooth continuous lines display a fit of the sum of two Gaussian distributions.

High-frequency noise in the calorimetric data was filtered out, after the experiment, by a fifth-order all-pole Butterworth filter with a normalized cutoff frequency of 8×10^{-2} Hz. The spikes of the experiments were obtained by searching the local maxima in the heat flux signal. The number of spikes larger than 23 μJ is 929 for the cooling run and 1518 for the heating run. The avalanche activity was measured as number of spikes per interval of 0.5 K. The temperature-dependent activity is shown in Fig. 4. The activity shows a single peak during the cooling experiment, two peaks are observed during the heating run. The enthalpy change occurs mainly during the low-temperature transformation while the spike activity is stronger at the high-temperature transformation. The avalanches were statistically analyzed and the exponent of the power-law probability $p(E) \sim E^{-\varepsilon}$ was determined (Fig. 5, top panel) using a maximum-likelihood analysis. An exponent $\varepsilon = 2.0 \pm 0.3$ was obtained for the cooling run. For the heating run, the signals for the two transformations were analyzed separately. An exponent $\varepsilon = 2.4 \pm 0.4$ was obtained for the low-temperature transformation and $\varepsilon = 2.2 \pm 0.3$ was obtained for the high-temperature transformation, albeit with very few peaks in the thermal curve.

In Cu-based shape-memory alloys an entropy change of ca. 1.3 J/K mol was predicted for systems transforming to the $18R$ phase and an entropy change of 1.6 J/K mol for systems transforming to the $2H$ phase [20]. Taking the fractions of both phases estimated from calorimetric measurements and

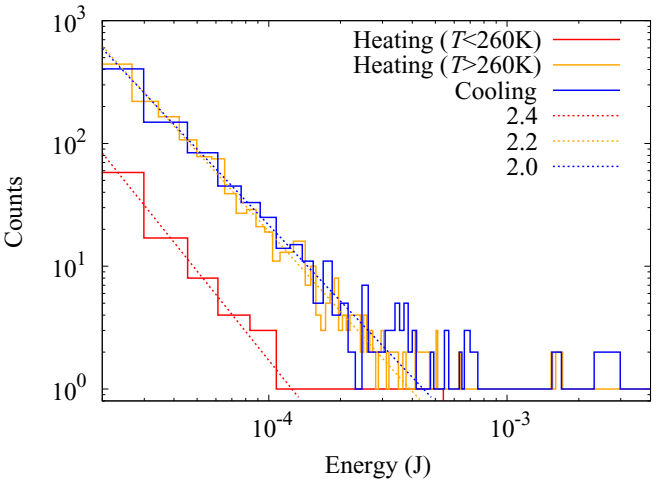

FIG. 5. Log-log plot of the distribution of energies (linear bins) of the spikes detected from calorimetric measurements. Data recorded during the heating run are split at $T = 260$ K separating the contributions to the activity observed in Fig. 4. Straight lines display best power-law fits to experimental data.

a common equilibrium temperature $T_0 \simeq 250$ K for both $\beta \leftrightarrow 18R$ and $\beta \leftrightarrow 2H$ transitions, we obtain that the heat exchanged at the transformation should be, $q \simeq 1.3$ (J/mol K) $\times 0.94 \times 250$ (K) $+1.6$ (J/mol K) $\times 0.06 \times 250$ (K) $=$ 329.5 J/mol, which is very close to the calorimetrically measured transformation enthalpy of 328 J/mol during the cooling run. This result is hence consistent with the interpretation that, on cooling, the transition occurs to a mixture of 94% $18R$ and 6% $2H$. The splitting of the reverse transitions under heating is a consequence of the fact that the transition to the $2H$ phase is known to occur with a much wider thermal hysteresis than the transition to the $18R$ phase [25,33].

An additional calorimetric experiment was performed to study the thermal hysteresis of the two transformations. First, the sample was cooled down to 200 K from room temperature (step 1); it was heated up to 260K (step 2) when the low-temperature transition appeared finished. The sample was then recooled to 220 K (step 3) and heated again to room temperature (step 4). DTA traces for this experiment are shown in Fig. 6.

The data for step 1 and step 2 are similar to those obtained in the initial experiments (see Fig. 3). Following the ideas previously described [22,23], a mixture of monoclinic $18R$ and orthorhombic $2H$ grows during the cooling transformation. The transition from monoclinic $18R$ to cubic β phase has been completed after step 2 and the sample contains a mixture of the cubic and orthorhombic phases.

When the sample is cooled again (step 3), a broad anomaly is found. The new transition starts at a higher temperature (by approximately 5 K) while the peak temperature of the heat flux does not change. Very few spikes occur in this experiment (around 20 events), which suggests that avalanches during the cooling transformation are due to the now-depleted cubic to orthorhombic transformation.

Finally, the sample is heated from 220 K to room temperature (step 4). Two slightly overlapped stages were found. The low-temperature transformation is smeared with no spikes. The high-temperature transformation shows a larger number

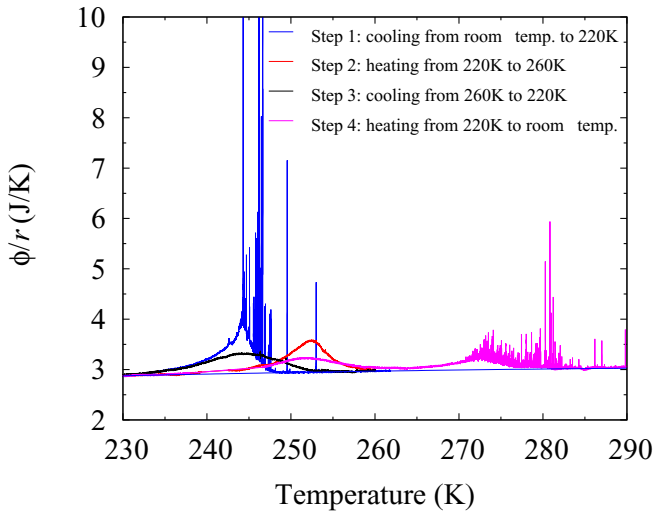

FIG. 6. Heat flux versus temperature for several runs: step1, cooling from room temperature to 220 K (blue line); step 2, heating from 220 K to 260 K (red line); step 3, cooling from 260 K to 220 K (black line); step 4, heating from 220 K to room temperature (magenta line).

of spikes (3712) which are superimposed to a broad smooth anomaly. This smeared anomaly was not previously observed in the first experiment. The total enthalpy balance is fulfilled as shown irrespective of the thermal history of the sample (Fig. 7.)

We recorded AE signals during heating and cooling with rates 5.5×10^{-3} K/s. AE rates are usually much faster than calorimetric rates, which are determined by the very slow response of the calorimeter. We started measurements at a high enough temperature of 320 K that ensures that the sample is fully in the β phase. The sample was then cooled to 220 K and subsequently heated from 220 K to 320 K. Figure 8 (top panel, blue curve) shows that during cooling significant AE activity was detected between 260 K and 230 K, with a maximum near 240 K. The AE activity peak is located in the same temperature interval where avalanches in the heat flux were found. Also in

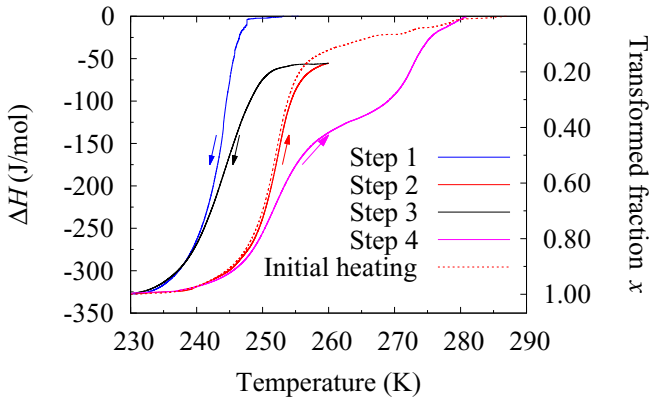

FIG. 7. Enthalpy excess (obtained from integration of calorimetric curves) versus temperature for several runs: step 1, cooling from room temperature to 220 K (blue line); step 2, heating from 220 K to 260 K (read line); step 3, cooling from 260 K to 220 K (black line); heating from 220 K to room temperature (magenta line). The dotted red line represents the enthalpy for the initial heating run.

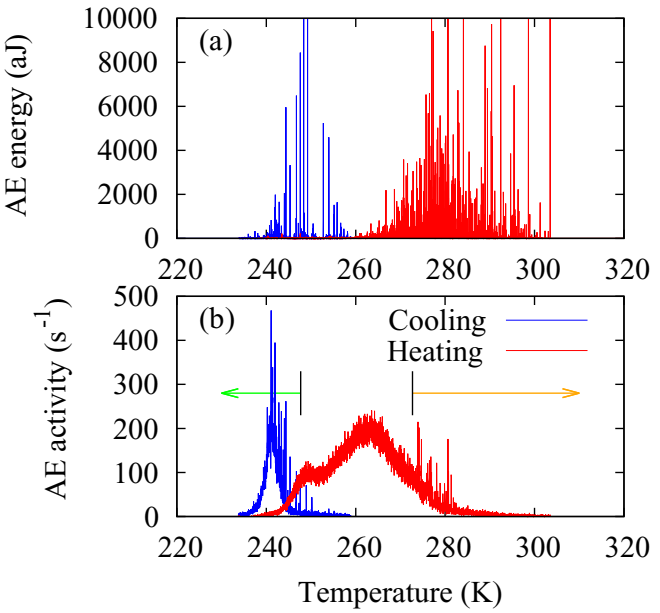

FIG. 8. (a) AE energy cumulated in bins of 2 s as a function of temperature during cooling from 320 K down to 220 K (blue) and subsequent heating up to 320 K (red). (b) AE activity recorded during the same runs (using also bins of 2 s). The arrows indicate the range for the analysis presented in Fig. 9(b).

agreement with calorimetry, the activity peak shows big spikes at the early stages of the transformation and becomes smoother at the late stages. In contrast, during heating AE appears in a very broad interval between 240 K and 300 K (see Fig. 8, top panel red curve). Two peaks were identified in this interval by calorimetry, while only one broad peak is seen in AE. When the AE energy is examined, instead of the AE activity, (see Fig. 8, top panel), a large amount of the energy dissipated by AE is associated with the big AE spikes while little energy is dissipated in the smoother transformations regions.

We show the distribution of energies of one complete set of AE signals during cooling and heating runs as log-log plot in Fig. 9(a). An approximate power-law distribution with

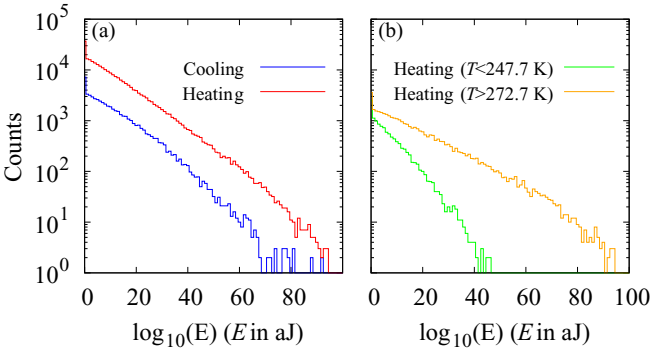

FIG. 9. (a) Log-log plot of the distribution of avalanche energies (in aJ) for complete cooling and heating runs. (b) Distribution of avalanche energies (in aJ) for signals detected in the temperature interval 230–250 K (corresponding to the $18R \rightarrow \beta$ transition) and 270–290 K (corresponding to the $2H \rightarrow \beta$ transition) respectively. The intervals are indicated in Fig. 8.

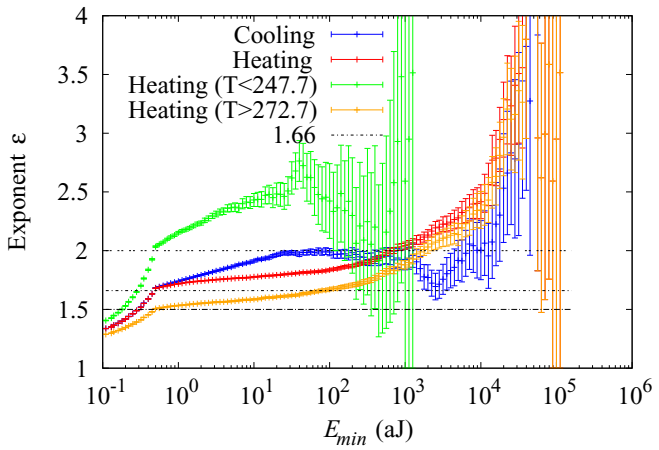

FIG. 10. Likelihood plots corresponding to the distributions shown in Figs. 8(a) and 8(b).

some exponential cutoffs is obtained over more than three decades. The corresponding characteristic exponents have been obtained using a maximum likelihood method, which consists of studying the behavior of the fitted exponent as function of a varying lower cutoff $E_{\min}$ (see, for instance, Ref. [34]). This analysis should lead to a plateau that defines the characteristic exponent. This is shown in Fig. 10. The plateau is not well defined but some region with small slopes appears. The exponent was estimated at the onset of the plateau as indicated by dashed lines in the likelihood curves in Fig. 10. The exponents obtained are $\varepsilon = 1.7 \pm 0.2$ for cooling and heating runs. We have further analyzed separately signals corresponding to the early $18R \rightarrow \beta$ and late $2H \rightarrow \beta$ stages during heating. The corresponding energy distributions are shown in Fig. 9(b) and the results of the maximum-likelihood analysis shown in Fig. 10. An energy exponent $\varepsilon = 2.0 \pm 0.15$ (green curve) is obtained for signals at the early stages while an exponent $\varepsilon = 1.5 \pm 0.15$ (orange curve) is estimated for later stages. These values are in excellent agreement with those predicted for $\beta \leftrightarrow 18R$ and $\beta \leftrightarrow 2H$ transitions, respectively [8].

The results of the RUS measurements are shown in Fig. 11. Cooling the sample leads to a decrease of the shear stiffness of the sample. Figure 11 shows data from two elastic RUS resonances. Both resonances show a weak but significant decrease of the shear modulus above 260 K and a strong dependence on the thermal history of the sample. First, cooling from room temperature to 220 K gives a well-defined transition at 242 K with significant softening below 280 K. The phase below 242 K is not static and shows strong thermal hardening under cooling. Subsequent heating from 220 K to 260 K leads to a much wider transition at 249 K. At 260 K the shear modulus has not recovered the stiffness of the virgin crystal during cooling. Repeated cooling from 260 K to 220 K recovers the transition at 242 K of the first cooling experiment. The data in the low-temperature phase are fully reproduced and show no thermal hysteresis. Second heating from 220 K to room temperature leads to elastic softening, which is further shifted to higher temperatures. The transition region is now very broad and the maximum damping and minimum shear modulus is around 254 K, which is well above the initial

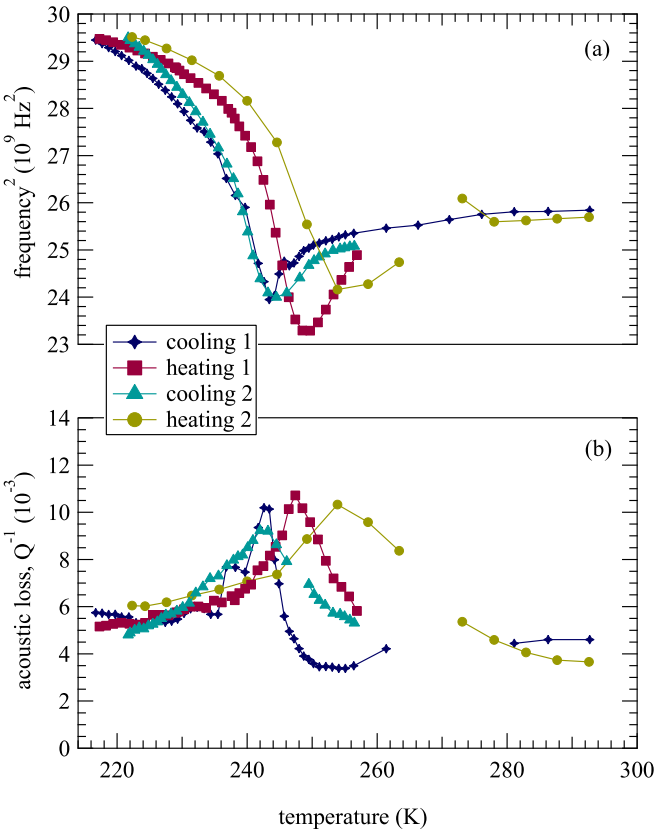

FIG. 11. RUS frequencies (a) and damping (b) during cooling and heating experiments. The sample was first cooled to 220 K, then heated to 260 K, recooled to 220 K and finally heated to room temperature. The minima in the squared RUS frequency and the maximum of the damping Q^{-1} are close to the transformation instability points, which show with thermal history. The gradual changes below 242 K show that the $18R$+$2H$ phase mixture is not athermal at low temperatures.

transition temperature of 248 K. The initial shear moduli are fully recovered above 280 K.

IV. DISCUSSION

The three experimental techniques disclose mechanisms of the thermal transformation of a Cu-Al-Ni shape-memory alloy on different length scales. Calorimetry measures the total transformation enthalpy and, additionally, detects avalanches as indication that the transformation contains non-smooth dynamics. This does not mean that the entire process is nonsmooth as much of the enthalpy is contained in a continuous background signal. In contrast, AE is a very sensitive technique to small changes of the local strain field, and thus very adequate to quantify avalanche dynamics. RUS measurements average over times that are much longer than the life times of avalanches [35]. RUS measures the overall elastic shear moduli of the sample, which includes both intrinsic softening/stiffening due to coupling of the order parameter with strain and extrinsic contributions dominated by the formation and change of twin and interfacial microstructures.

First cooling of Cu-Al-Ni leads to a main transformation event near 242 K, which is observed by all techniques. Calorimetry reveals that the resulting low-temperature form

is a phase mixture of $18R$ and $2H$. The proportions between these phases is strongly biased toward the $18R$ phase, i.e., 94%. In contrast, the AE signal is biased towards the transformation into the $2H$ phase. The RUS spectra show an overall elastic softening, which reaches a maximum at the transition point. The details of the softening are unusual for martensites, however, where the shear modulus remains temperature independent once the martensite is formed. This archetypal behavior was reported, e.g., for $Cu_{74.08}Al_{23.13}Be_{2.79}$ [36]. The microstructure of the martensite phases in Cu-Al-Ni still changes at low temperatures so that the athermal behavior is never established for these phase transitions. This observation qualifies the term athermal: at 242 K the β phase transforms into $18R$ and $2H$ in a narrow temperature interval while the microstructure of the phase mixture changes under further cooling. During this thermal adaptation [37] no AE signals or jerky heat fluxes are found. This means that the proportions between the $2H$ and $18R$ phases do not change in any measurable way but that the twin microstructures do. The thermal hardening of the shear moduli is fully reproducible on cooling but not on heating where we also find a significant thermal hysteresis. This indicates that the elastic hardening and increase of the elastic damping (as expressed by Q^{-1}) during cooling relates to gradual domain wall freezing with an extremely broad excitation spectrum. Such thermal behavior is commonly observed in ferroelastic materials [38,39].

AE is expected to be associated with the amount of transformation hysteresis [40] so that the AE results can be understood if a transformation to two martensitic phases $18R$ and $2H$ occurs simultaneously during cooling. During heating these two martensites retransform differently. At the early stages, the $18R$ phase retransforms to the parent phase (and possibly some $2H$) with a weak hysteresis and thus with AE carrying very little dissipated energy. At higher temperature, the $2H$ phase retransforms under the emission of very intense AE signals. The main AE energy near 280 K is then associated with the transforming between the small amount of $2H$ and β.

We now return to the discussion of energy exponents. The pure phase transitions $\beta \leftrightarrow 2H$ and $\beta \leftrightarrow 18R$ show relatively good power-law distributions of avalanche energies in both heat flux and AE measurements. The exponents for the individual transformations were identified under heating. AE measurements render clearly different exponents, namely $\varepsilon = 2$ ($\beta \leftrightarrow 18R$) and $\varepsilon = 1.5$ ($\beta \leftrightarrow 2H$). The exponent for the majority transformation $\beta \leftrightarrow 18R$ is far removed from the expected mean field value[4] while the lower value may coincide with mean-field theory if the boundary conditions are carefully chosen [41]. The phase mixture shows an intermediate exponent $\sim$1.7 in AE. The errors in the exponents determined from calorimetric measurements are large and discrimination of different exponents is less clear. In fact, heat flux measurements render in general slightly larger exponents than AE measurements. In our case the discrepancies between calorimetric and AE determination of the exponents seem to be a consequence of a relatively bad statistics in the case of calorimetric measurements. It is worth noting that the number of detected signals is at least one order of magnitude larger in the case of AE measurements. Nevertheless, we should not ignore the fact that AE and calorimetric techniques enable avalanche detection in very different energy intervals. The fact that the obtained exponents are so similar reinforces the idea of scale invariance of the avalanche process.

An interesting issue to be discussed in some more detail is the different energy exponents estimated for the $\beta \leftrightarrow 18R$ and $\beta \leftrightarrow 2H$ transitions. It has been suggested that these exponents depend essentially on variant multiplicity, which is given by the number of equivalent structural domains that can occur at the transitions. That is, on the ratio between the symmetry operations in the parent and martensitic phases. From this perspective, systems with different variant multiplicity should belong to different universality classes. The idea behind this point of view is that by increasing variant multiplicity, the system is able to find more paths connecting high and low symmetry phases. Thus, as variant multiplicity increases the probability of large events should decrease compared with the probability of small ones, which should give rise to a larger critical exponent. The variant multiplicity is 6 for the $\beta \rightarrow 2H$ and 12 for the $\beta \rightarrow 18R$ transition. This coincides with a change of energy exponents from $\varepsilon = 1.5$ ($\beta \leftrightarrow 2H$) to $\varepsilon = 2$ ($\beta \leftrightarrow 18R$) so that an increase in the multiplicity also leads to an increase of the exponent.

The increase of multiplicity has another effect; it can increase the smoothness of the transition. If the geometrical transformation occurs using a greater number of intermediate stepping stones it can occur with fewer or no avalanches on a local stage. In Cu-Al-Ni we find that the majority $\beta \leftrightarrow 18R$ transformation is much smoother than the $\beta \leftrightarrow 2H$ transformation although the latter involves only a very small fraction of the sample.

A simple model has recently been proposed based on branching random processes to deal with the change of critical exponent with variant multiplicity [42]. The model assumes that the martensitic microstructure evolves by means of the successive growth of thin martensitic plates, which can propagate in given directions, which correspond to habit planes, until they encounter an existing plate. An AE event (avalanche) is associated with the formation of each plate. The number of directions determines variant multiplicity. The model reproduces scale invariance of avalanches during the martensitic transitions and show that the critical exponent characterizing the avalanche size distribution decreases with variant multiplicity (growth directions) increases.

Finally, we conclude that avalanche criticality in martensitic transitions is largely determined by the symmetry change at the transition and is independent of details such as the existence of internal stresses that may influence the transition path.

ACKNOWLEDGMENTS

We acknowledge financial support from the Spanish Ministry of Science (Mat2013-40590-P and MAT2015-69777-REDT). E.K.H.S. is grateful to EPSRC (Grant No. EP/K009702/1) and the Leverhulme Foundation (Grant No. RPG-2012-564) for support. RUS facilities have been established and maintained in Cambridge through grants from the Natural Environment Research Council and the Engineering and Physical Sciences Research Council of Great Britain to MAC (NE/B505738/1, NE/F17081/1, EP/I036079/1).

[1] *Shape Memory Materials*, edited by K. Otsuka and C. M. Wayman (Cambridge University Press, Cambridge, 1998).

[2] F. J. Pérez-Reche, M. Stipcich, E. Vives, L. Mañosa, A. Planes, and M. Morin, Phys. Rev. B **69**, 064101 (2004).

[3] E. K. H. Salje, X. Ding, Z. Zhao, T. Lookman, and A. Saxena, Phys. Rev. B **83**, 104109 (2011).

[4] E. K. H. Salje and K. A. Dahmen, Ann. Rev. Cond Matter. Phys. **5**, 233 (2014).

[5] F. J. Pérez-Reche, L. Truskinovsky, and G. Zanzotto, Phys. Rev. Lett. **101**, 230601 (2008).

[6] E. Vives, D. Soto-Parra, L. Mañosa, R. Romero, and A. Planes, Phys. Rev. B **80**, 180101(R) (2009).

[7] L. Zhang, E. K. H. Salje, X. Ding, and J. Sun, Appl. Phys. Lett. **104**, 162906 (2014).

[8] A. Planes, L. Mañosa, and E. Vives, J. Alloys Compd. **577**, S699 (2013).

[9] E. Faran, H. Seiner, M. Landa, and D. Shilo, Appl. Phys. Lett. **107**, 171601 (2015).

[10] A. Planes, J. L. Macqueron, M. Morin, and G. Guénin, Phys. Status Solidi A **66**, 717 (1981).

[11] K. Yoshida, S. Kihara, and K. Sakamaki, *Proceedings of the International Conference on Solid-Solid Phase Transformations'99 (JIMIC-3)*, edited by M. Koiwa, K. Otsuka, and T. Miyazaki (The Japan Institute of Metals, 1999), pp. 919–922.

[12] T. Yasuda, B. Pang, H. Nishio, and K. Yoshida, Mater. Trans. **52**, 397 (2011).

[13] K. Otsuka, A. Saxena, J. Dengac, and X. Ren, Philos. Mag. **91**, 4514 (2011).

[14] N. Suresh and U. Ramamurty, J. Alloys Compd. **449**, 113 (2008).

[15] Ş. N. Balo and N. Sel, Thermochim. Acta **536**, 1 (2012).

[16] A. Ibarra, J. San Juan, E. H. Bocanegra, and M. L. Nó, Acta Mater. **55**, 4789 (2007).

[17] P. Sedlák, H. Seiner, M. Landa, V. Novák, P. Šittner, and L. Mañosa, Acta Mater. **53**, 3643 (2005).

[18] B. Graczykowski, P. Biskupski, B. Mroz, S. Mielcarek, M. L. Nó, and J. San Juan, Smart Mater. Struct. **19**, 015010 (2010).

[19] T. B. Massalski and U. Mizutani, Prog. Mater. Sci. **22**, 151 (1978).

[20] A. Planes and L. Mañosa, Solid State Phys. **55**, 159 (2001).

[21] E. Obradó, L. Mañosa, and A. Planes, Phys. Rev. B **56**, 20 (1997).

[22] J. VanHumbeeck, D. Van Hulle, L. Delaey, J. Ortín, C. Seguí, and V. Torra, Trans. Jpn. Inst. Met. **28**, 383 (1987).

[23] C. M. Friend, J. Ortín, A. Planes, L. Mañosa, and M. Yoshikawa, Scr. Metall. Mater. **24**, 1641 (1990).

[24] V. Recarte, R. B. Pérez-Saez, E. H. Bocanegra, M. L. Nó, and J. San Juan, Mater. Sci. Eng. A **273-275**, 380 (1998).

[25] K. Otsuka, H. Sakamoto, and K. Shimitzu, Acta metall. **27**, 585 (1979).

[26] E. K. H. Salje, Annual Rev. Mater. Sci. Res. **42**, 265 (2012).

[27] F. J. Pérez-Reche, E. Vives, L. Mañosa, and A. Planes, Phys. Rev. Lett. **87**, 195701 (2001).

[28] M. C. Gallardo, J. Jiménez, and J. del Cerro, Rev. Sci. Instrum. **66**, 5288 (1995).

[29] J. del Cerro, F. J. Romero, M. C. Gallardo, and J. Jiménez, Thermochim. Acta **343**, 89 (2000).

[30] A. Migliori and J. L. Sarrao, *Resonant Ultrasound Spectroscopy* (Wiley, New York, 1997), p.201.

[31] A. Migliori and J. D. Maynard, Rev. Sci. Instrum. **76**, 121301 (2005).

[32] R. E. A. Mcknight, M. A. Carpenter, T. W. Darling, A. Buckley, and P. Taylor, Am. Min. **92**, 1665 (2007).

[33] J. Ortín, L. Mañosa, C. M. Friend, A. Planes, and M. Yoshikawa, Philos. Mag. A **65**, 461 (1992).

[34] H. Bauke, Eur. Phys. J. B **58**, 167 (2007).

[35] E. K. H. Salje, X. Wang, X. Ding, and J. Sun, Phys. Rev. B **90**, 064103 (2014).

[36] E. K. H. Salje, H. Zhang, H. Idrissi, D. Schryvers, M. A. Carpenter, X. Moya, and A. Planes, Phys. Rev. B **80**, 134114 (2009).

[37] D. D. Viehland and E. K. H. Salje, Adv. Phys. **63**, 267 (2014).

[38] W. Schranz, P. Sondergeld, A. V. Kityk, and E. K. H. Salje, Phys. Rev. B **80**, 094110 (2009).

[39] A. V. Kityk, W. Schranz, P. Sondergeld, D. Havlik, E. K. H. Salje, and J. F. Scott, Phys. Rev. B **61**, 946 (2000).

[40] E. Bonnot, E. Vives, L. Mañosa, A. Planes, and R. Romero, Phys. Rev. B **78**, 094104 (2008).

[41] J. T. Uhl, S. Pathak, D. Schorlemmer, X. Liu, R. Swindeman, B. A. W. Brinkman, M. LeBlanc, G. Tsekenis, N. Friedman, R. Behringer, D. Denisov, P. Schall, X. Gu, W. J. Wright, T. Hufnage, A. Jennings, J. R. Greer, P. K. Liaw, T. Becker, G. Dresen, and K. A. Dahmen, Sci. Rep. **5**, 16493 (2015).

[42] J. C. Ball, P. Cesana, and B. Hambly, MATEC Web of Conferences **33**, 02008 (2015).